Special Section: Multiscale Mapping
Vadose Zone Journal

Modeling Local Scaling Properties for Multiscale Mapping

Qiuming Cheng*

Mapping surface soil properties and estimating soil parameters with multiresolution data has been significantly advanced by newly developed multiscale mapping technologies, which incorporate the concept and models of scaling analysis in data processing. This study was conducted to develop a new multiscale mapping technique on the basis of a power-law model characterizing local singularity of exploratory data for mapping surface soil properties. A field with singularity due to self-organization or self-similarity properties of the underlying processes can be modeled by multifractal models. These types of data may not have the statistical stationary property required by ordinary geostatistical mapping techniques. The new mapping technique utilizes a scaling property for data interpolation and for downscaling image processing. The inputs, either point data or an image, can be separated into a nonsingular background component for estimation purposes and an anomalous component of singularity for multiscale high-pass filtering purposes. When used for the purpose of data interpolation, this new method assigns weights for data interpolation by taking into account not only the distance between neighborhood points but also local structures and singularity of the field. The results of application of the method to a data set of geochemical concentration values of Ag from 1172 lake sediments in the Gowganda area of Ontario, Canada, have delineated favorable target areas with strong singularity of Ag concentrations caused by mineralization in lake sediments.

Abbreviations: GIS, geographic information systems; IDW, inverse distance weighting.

The technology for mapping surface soil properties and estimating soil properties has been significantly advanced by developments of various types of new space-borne, airborne, and ground-based sensor technologies. In some areas, however, due to time and cost constraints, mapping techniques with point-based field observation and measurement is still commonly used. Recently, a sufficient amount of high-precision data have become available in mapping properties of soils; for example, hyperspectral and multispectral remote sensing images with multiple spatial resolutions are available for mapping soil properties including humidity, surface roughness, surface crusting, and water storage (Sullivan et al., 2005). To investigate the scale dependence of these types of estimation often requires multiple-resolution images. Representation of such images at multiple scales can be effective for information extraction and map processing. Digital maps and digital map processing techniques such as geographic information systems (GIS) and remote sensing image processing systems have made this possible not only for visualization purposes for maps of various forms and at multiple scales but also for quantitative digital image processing to analyze data and extract new information. For example, fusing images with high frequency but low spatial resolution and images with low frequency but high spatial resolution to generate new images with both high frequency and high spatial resolution involves downscaling image processing. Image filtering techniques, commonly used for digital image processing, enhance some features of interest and reduce the influences of other features considered as noise. For example, for the purpose of estimation of soil properties, high-frequency variability of the data caused by local features may be considered noise that must be removed from the estimation; however, if the purpose of image processing is to detect anomalies caused by special features such as water contamination, soil erosion, surface crusting, and surface roughness, then the high-frequency variability of the images must be retained. The method introduced here is useful for mapping these types of properties by separating the background values with local singularity removed for estimation of soil properties from anomalous values showing local singularity for detection of local variability of soil properties.

The development of fractal and multifractal theory has provided the means for describing the regularity of change of spatial patterns as map scale changes (Mandelbrot, 1972, 1974; Feder, 1988). The scale-invariant property (scaling) has not only been observed from many types of map patterns but also proved to be useful for characterizing the variability reflected in a map. Several multifractal models have been used in geoscience to analyze maps

State Key Laboratory of Geological Processes and Mineral Resources, China Univ. of Geosciences, Wuhan 430074, Beijing 100083, China; and Dep. of Earth and Space Science and Engineering and Dep. of Geography, York Univ., 4700 Keele St., Toronto, ON M3J 1P3, Canada. Received 13 Feb. 2007. *Corresponding author (qiuming@yorku.ca).

Vadose Zone J. 7:525–532
doi:10.2136/vzj2007.0034

© Soil Science Society of America
677 S. Segoe Rd. Madison, WI 53711 USA.
All rights reserved. No part of this periodical may be reproduced or transmitted in any form or by any means, electronic or mechanical, including photocopying, recording, or any information storage and retrieval system, without permission in writing from the publisher.

or patterns observed on the surface or near the surface of the Earth or remotely sensed from space (Frisch and Parisi, 1985; Grassberger, 1983; Hentschel and Procaccia, 1983; Badii and Politi, 1984, 1985; Halsey et al., 1986; Schertzer and Lovejoy, 1987; Evertsz and Mandelbrot, 1992; Agterberg, 1995, 2005; Cheng et al., 1994; Cheng, 2007b).

Mapping a feature of interest of an area from point observation data often involves data interpolation to assign values at the locations where no measurements are being made. The assumption taken for most data interpolation methods is that the values at known locations are associated with the values at the unknown locations where the values must be interpolated. The association between the values at different locations is usually related to the distance between the locations. There have been a number of techniques developed under this assumption for data interpolation.

Three common interpolation techniques have been implemented in ArcGIS software (ESRI, 2000), called the spline method, inverse distance weighting, and kriging. The spline method fits a surface to point data with a predetermined spline function with a certain degree of smoothness, and assumes that the values for known and unknown locations follow the same mathematical model and thus can be fitted with the same type of function. The main advantage of the spline method is the ability to generate deterministic surfaces from only a few sample points. The main disadvantage of this method is that the spline method applies a predetermined function that may not fit the real shape of the data.

Inverse distance weighting (IDW) is a moving-average technique based on the assumption that the values of the neighboring observations contribute more to the interpolated values than the values of distant observations. The influence of the data at a known point on the interpolation is inversely related to the distance between the known location and the unknown location where values must be estimated. The inverse distance decay rate is determined by a predetermined function parameter. The advantage of the IDW method is that it is intuitive and implementation is straightforward. Its main disadvantage is related to the determination of the weights based only on the location and ignoring the variance of the property of the values themselves.

Kriging is a more sophisticated method that assigns weights for the location of points by taking into account not only the distance between the known and unknown locations but also the spatial association of the values, which is characterized by a semivariogram function. Kriging is a core subject in the field of geostatistics, a discipline primarily dedicated to mapping with spatial statistical and stochastic models. Kriging has long been applied in the geosciences for data estimation and simulation. The semivariogram is a function measuring the spatial variance between values at locations separated by a distance (Journel and Huijbregts, 1978). The semivariogram has also been used for characterizing the structural property of a landscape. As a second-order moment statistic, the semivariogram requires the data to have an intrinsic stationary property. Assuming that the data come from a random process with a constant mean, and a semivariogram that only depends on the distance and direction separating any two locations independently, one can fit a semivariogram with a mathematical model that can be used as a global model for assigning associations to any two locations. This is needed to form the normal equations from which the weights can be obtained for those locations involved for moving averaging in kriging. The major advantage of kriging in comparison with IDW is estimating weights for locations based not only on the distance between separated locations but also on the global semivariogram model fitted to the data. One of the main drawbacks of this method, however, is that it requires data with a stationary property. The stationarity condition may not be met by most exploratory data with anomalies and extreme values.

A common drawback of the moving average methods, including IDW and kriging, is that these methods do not take into account the local properties of the data. The method introduced here attempts to overcome the preceding drawbacks by incorporating local singularity into the basic model of moving averaging. A power-law model is established for quantification of local singularity. According to this method, the weights for the moving average are assigned on the basis of the local scaling property of the data. The application of this method is demonstrated using a data set of geochemical element concentration values in lake sediment samples from the Gowganda area of northeastern Ontario. Similar applications can be used to map surface soil properties such as surface crusting, roughness, erosion, and soil moisture contents.

Materials and Methods

Study Area and Material Descriptions

The study area is located in the Gowganda–Cobalt area of northeastern Ontario and is mainly underlain by the Proterozoic rocks of the Huronian Supergroup (Fig. 1). The Huronian rocks in the area are composed of the Lorrain Formation (quartz sandstone, minor conglomerate, and siltstone) and the Gowganda Formation (mostly diamictite and argillite). Archean-aged supracrustal rocks composed of intercalated felsic to mafic metavolcanic flows with minor ultramafic to mafic rocks underlie approximately 8% of the study area. Felsic intrusive rocks with variable composition cover approximately 12% of the area (Hamilton, 1997). Diabase intrusions as sills and steeply dipping dikes and plugs, known as the Nipissing diabase, are quite abundant and intrude the Archean basement and most of the Huronian rocks. Approximately 50% of the study area is covered by exposed bedrock or relatively thin overburden. The Quaternary geology of the area is mostly characterized by ice-contact stratified drift with associated sandy glaciofluvial deposits. The dominant ice flow is believed to be an older southwest flow superimposed by a younger south–southeast flow (Hamilton, 1997; Panahi et al., 2003).

The Silver Deposits

The Ag sulpharsenide vein deposits in the Cobalt and Gowganda areas of northeastern Ontario occur along the north and northeastern margins of the Cobalt Embayment. The vein systems are generally fault controlled, with mineralization occurring adjacent to or within the Nipissing diabase sills, in close proximity to the Huronian–Archean unconformity (Andrews et al., 1986). The chemistry of the veins indicate Ag, As, Co, Pb, and rare earth elements among the components introduced with the hydrothermal fluids.

Lake Sediment Data

A total of 1172 lake sediment samples were collected from an area of 2700 km^2 by the Ontario Geological Survey in 1997

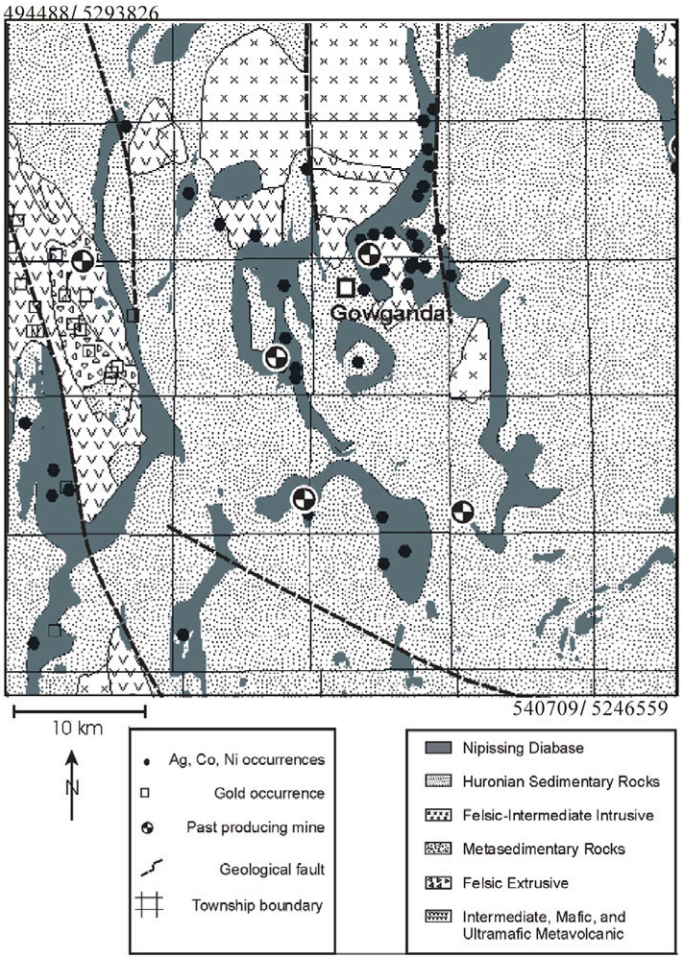


FIG. 1. Simplified geology of the Gowganda area.

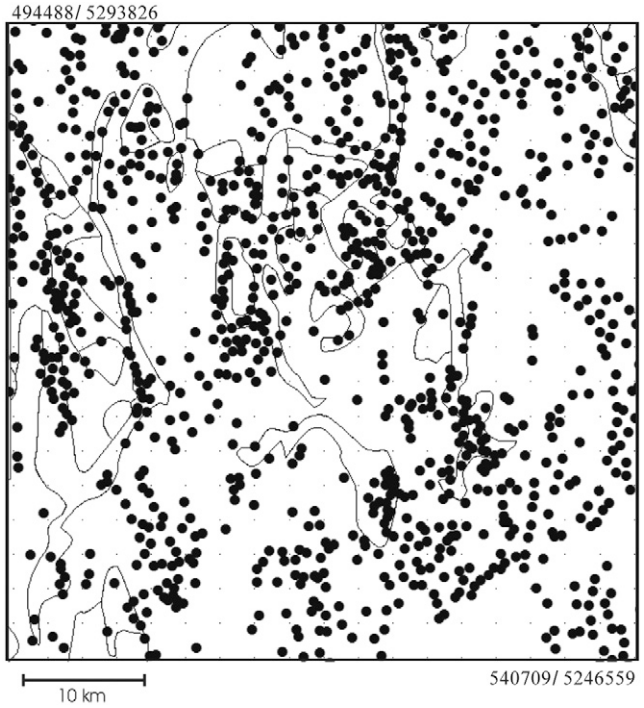


FIG. 2. Locations of 925 lake sediment samples from the Gowganda area (data from Hamilton, 1997).

(Hamilton, 1997), providing a relatively uniform coverage and regular distribution. To avoid edge effects, a smaller area with 925 samples was chosen as the actual area for mapping. The sample locations are shown in Fig. 2. Lake sediment samples were analyzed by instrumental neutron activation analysis for Au, As, Na, and Br and by inductively coupled plasma–mass spectrometry for another 51 elements. Quality control procedures and reports are found in Hamilton (1997). This data set was used by Panahi et al. (2003) for mapping the mineral potential for Ag and Au in the area.

Spatial Associations, Stationarity, and Singularity

To discuss spatial association vs. singularity of map values, we will first introduce several notations and concepts of point location, point data, pixel, and pixel value. In the GIS context, a point is represented as a location with two coordinates in vector format or as a pixel in raster format. Points have no size but pixels do. Raster maps are built up with pixels and the pixel size determines the spatial resolution of the map. The conversion from point data (vector data) to pixel value (raster data) is an upscaling process. Assigning values to pixels from point data often involves data interpolation. How reasonable the estimated values are for the pixel depends on the complexity of the pixel values and how many point data can be used to calculate the pixel values. Differentiating these two types of information is helpful for understanding the concepts of spatial association and singularity. The former is usually calculated directly from the point data using the distance between sample locations, whereas the latter is calculated from sets of pixels (or other shapes of windows) with multiple sizes. Denote the value at point location x as $Z(x)$ and the value of a pixel of size ε centered at location x as $\mu(x, \varepsilon)$. The distance between two points x and y or between pixels centered at x and y can be denoted as $||x - y||$. The unit of the distance can be a metric unit or pixels. These notations help us to discuss the indices of spatial association and local singularity.

Spatial Association

The spatial association involved in data interpolation often represents a type of statistical dependency of values at separate locations. If the value at a location is considered to be a realization of a so-called regionalized random variable, the spatial association or variability can be measured by means of a semivariogram, which can be expressed as follows (Journel and Huijbregts, 1978):

$$2\gamma(x,\mathbf{h}) = \left\langle \left[Z(x) - Z(x+\mathbf{h}) \right]^2 \right\rangle \quad [1]$$

where $\gamma(x, \mathbf{h})$ is a function of vector distance $\mathbf{h}$ separating locations x and $x + \mathbf{h}$, and $< >$ is the expectation. The semivariogram measures the symmetrical variability between $Z(x)$ and $Z(x + \mathbf{h})$. Under an assumption of second-order stationarity, the semivariogram Eq. [1] becomes a function of $\mathbf{h}$ independent of location x. This strong assumption of the regionalized random variable is generally required in kriging. The function Eq. [1] has been commonly used for structural analysis and for interpolation in geostatistics (Journel and Huijbregts, 1978). It has also been applied for texture analysis in image processing (Herzfeld, 1993; Herzfeld and Higginson, 1996; Atkinson and Lewis, 2000).

Singularity

The concept of singularity is used for characterizing the anomalous behaviors of singular physical processes that often result in anomalous amounts of energy release or material accumulation within a narrow spatial–temporal interval (Cheng, 2007a). Examples of singular processes include cloud formation (Schertzer and Lovejoy, 1987), rainfall (Veneziano, 2002), hurricanes (Sornette, 2004), flooding (Malamud et al., 1996), landslides (Malamud et al., 2004), and earthquakes (Turcotte, 1997). In general, the final products of these nonlinear processes can be modeled as fractals or multifractals (Cheng and Agterberg, 2008). Mineralization processes and oil- and gas-forming processes in the subsurface of the Earth could result in deposits or oil and gas fields characterized by high concentrations of metals, or oil and gas with fractal or multifractal properties (Cheng and Agterberg, 1996; Agterberg, 1995; Mandelbrot, 1989; Cheng, 2006; Xie and Bao, 2004). Outcomes of such processes are often characterized by positively skewed frequency distributions with Pareto upper-value tails. The largest values may be extreme events. Mineralization and the formation processes of oil and gas can be considered singular processes due to the large amounts of material accumulation and element enrichment. A simple way to test singularity in the multifractal context is to check how the statistical behavior varies as the measuring scale changes. For example, in some locations the mean values of pixels at different resolutions might be independent of the size of the pixel (small pixel sizes) within which the values are averaged. In other cases, the mean value might proportionally depend on pixel size. We call the former case *nonsingular* background and the latter *singular* component. The singularity property has been commonly observed in geochemical and geophysical quantities (Cheng et al., 1994; Cheng, 1997, 1999a, 2000). Taking the notation of the multifractal model, the singularity index $\alpha(x)$ is related to the measure $\mu(x, \varepsilon)$, defined for a pixel centered at location x of linear size ε, $\Omega(x, \varepsilon)$, as

$$\langle \mu(x,\varepsilon) \rangle = c\varepsilon^{\alpha(x)} \quad [2]$$

where c and $\alpha(x)$ are independent of ε. In case of soil geochemical data, $\mu(x, \varepsilon)$ can be defined as the amount of element concentration in the soil within an area of size ε. If a geochemical map is considered to be a realization of a regionalized random variable or random multiplicative cascade multifractal processes, then the singularity index $\alpha(x)$ may exist at the pixel scale rather than at the point scale. Due to the nugget effect, the density value ρ may not exist at a point location; for example, repeat sampling at the same location may give different values. In this case, average values within a pixel area should be applied. Therefore, $\alpha(x)$ becomes an approximation (represented as $\sim$) of singularity of values in a small area (Cheng, 2007b). For convenience but without losing generality, we will introduce a density function $\rho(x, \varepsilon)$ as

$$\langle \rho(x,\varepsilon) \rangle = \langle \mu(x,\varepsilon) \rangle / \varepsilon^{E} \sim c\varepsilon^{\alpha(x)-E} \quad [3]$$

where E is the dimension of the pixel $\Omega(x, \varepsilon)$ (E = 2 for a two-dimensional soil map). The value of the singularity $\alpha(x)$ varies within a finite range from α_{min} to α_{max}. The index $\alpha(x)$ can be estimated by the least squares method to fit a straight line to a set of values of $\mu(x, \varepsilon)$ against ε in log–log space. This can be done directly from the original point sample data; therefore, it is not affected by the smoothing of interpolation. The values $\alpha(x)$ and $\log(c)$ can be taken as the slope and the intercept of the straight line, respectively. The standard error and correlation coefficient involved in the estimation can be calculated from the least squares fitting and these indices can be used for evaluating whether power-law relationships Eq. [2] and [3] exist. The power-law relations Eq. [2] and [3] usually hold true for a certain range of pixel sizes, denoted as $[\varepsilon_{min}, \varepsilon_{max}]$, and the singularity index is the average value for the smallest pixel with the size of ε_{min}. The singularity index estimated from Eq. [3] has the following properties (Cheng, 1999a):

1. α = E, iff $\rho(x, \varepsilon) \sim$ constant, independent of pixel size ε.
2. α < E, iff $\rho(x, \varepsilon) \sim c\varepsilon^{\alpha-E}$ is a decreasing function of ε, which normally implies the "convex" property of $\rho(x, \varepsilon)$ at location x.
3. α > E, iff $\rho(x, \varepsilon) \sim c\varepsilon^{\alpha-E}$ is an increasing function of ε, which indicates the "concave" property of $\rho(x, \varepsilon)$ at location x.

Cases 2 and 3 correspond to singular situations in which the density function $\rho(x, \varepsilon) \to \infty$ or $\rho(x, \varepsilon) \to 0$ as $\varepsilon \to 0$. In the case of $\rho(x, \varepsilon) \to \infty$, it implies that within the pixel of size ε there is an anomalously high density of element concentration. This index (α) can be used as a measure characterizing the structural property of measure $\rho(x, \varepsilon)$ with pixel size ε. It needs good data coverage for accurate estimation of the singularity index at a small scale. This singularity index has been used for texture analysis during remote sensing image processing (Cheng, 1997, 1999b), in multifractal interpolation of geochemical concentration values for mineral exploration (Cheng, 1999a, 2000, 2001), and in well log curve reconstruction (Li and Cheng, 2001).

Distribution of the Singularity Index

The singularity index usually has finite values around E. For a conservative multifractal measure, the dimension of the set with $\alpha(x) = E$ is close to E (box-counting dimension), which means that the areas on a soil map with continuous background values occupy the greatest part of the map. The dimensions of the other areas with $\alpha(x) \neq E$ are given by the fractal spectrum function $f(\alpha) < E$ (Cheng, 1999a). This implies that the areas with singular values (anomalies) are relatively small in comparison with the areas with nonsingular values (background values). Based on a statistical point of view, the majority of values on the soil map where $\alpha(x) \sim E$ follows either normal or lognormal distributions, whereas the extreme values on the map with singularity $\alpha(x) \neq E$ may follow Pareto distributions. Kriging has been a common practice in data interpolation and is able to remove the samples with extreme values from the input data. For exploration purposes, however, the removal of the singular samples will smooth off local variability that may carry valuable information for anomaly identification. Most ordinary statistics techniques requiring the assumption of a normal (or lognormal) distribution of values may not be effective for processing exploratory data with extreme value distributions.

Scaling and Interpolation

The scaling property has been commonly observed in various types of patterns in the geosciences and used for prediction and estimation purposes, which has attracted as a great deal of

attention. A statistical property derived at one scale may be used to estimate the property at another scale (Agterberg, 2005). A data interpolation process that estimates values for small pixels without observation of the values available in surrounding locations can be considered a type of downscaling process. How to apply the scaling property in the process is obviously of general interest. The multifractal interpolation method developed by Cheng (1999a, 2000) for construction of curves (one-dimensional problem) and surfaces (two-dimensional problem) on the basis of point observations provides an example of using the scaling properties of map data for data interpolation. Here we briefly introduce the mathematical model of the method.

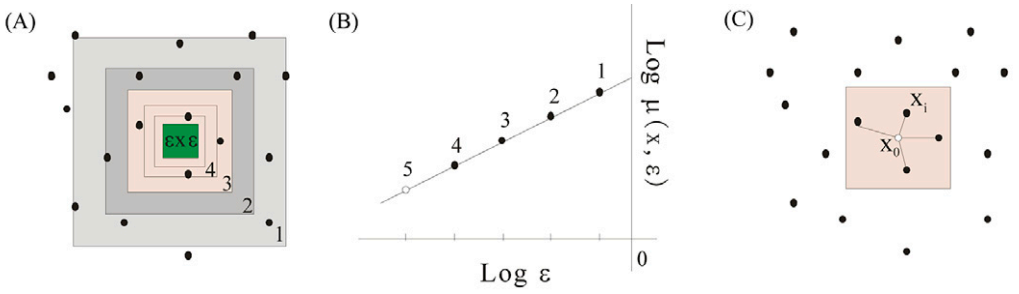


FIG. 3. Illustrations showing the processes of the downscaling interpolation Eq. [5] introduced here and the ordinary moving averaging model Eq. [4]: (A) boxes with variable sizes (1–4) were used to calculate the average values from point data (solid dots), while the box labeled εxε is a smaller pixel for which the average value was estimated using Eq. [5]; (B) a plot showing the relationship between the average element concentration values $\mu(x, \varepsilon)$ and box size ε at a log–log scale (solid dots represent the calculated values and the circle for the value to be estimated from Eq. [5]); and (C) the value estimated from neighbor point data to the center using Eq. [4].

Equation [3] shows that the average density function defined in a pixel size ε centered at a given location x follows a power-law relationship with the scale unit (pixel size ε). This relation shows a simple situation of the isotropic scaling property of pixel value. In a more complex situation when the scaling is anisotropic, variable window shapes should be used (Cheng, 2004, 2006). Here we will only deal with the isotropic scaling case, so squares for windows are applicable. The exponent $\alpha(x) - E$ characterizes the local singularity of the function—how the value changes as the scale unit decreases. At the singular location $\alpha(x) \neq E$, the density is dependent on the scale unit. In this case, the constant c becomes a useful quantity independent of pixel size and remains unchanged when pixel size reduces. This value of c ($c = \mu/\varepsilon^{\alpha}$) can be considered as the measure of the density $\rho(x, \varepsilon)$ in the space of $\alpha(x)$ dimension; for example, if μ stands for metal weight (g) in an area of linear size ε (cm), then c has the unit $(g/cm)^{\alpha}$. It becomes the ordinary density value in nonsingular locations where $\alpha = 2$. This decomposition is reasonable from the point of view of the Lebesgue decomposition theorem, which ensures that any complex measure decomposes into an absolutely continuous measure and a singular measure (Rudin, 1988). Local singularity can also be characterized in a time series signal by the wavelet transform method and is related to the Hölder exponent or Lipschitz exponent (Arneodo et al., 1992, 1995, 1998).

If we choose a given pixel size ε_0 in Eq. [3] at which the value of $\rho(x, \varepsilon_0)$ is calculated as the average density value of the pixel, then the value for any smaller pixels with size $\varepsilon < \varepsilon_0$ can be determined by $\rho(x, \varepsilon) = (\varepsilon/\varepsilon_0)^{\alpha(x)-E}\rho(x, \varepsilon_0)$. This property can be used for downscaling interpolation. For example, we can first estimate the average value $\rho(x, \varepsilon_0)$ at a resolution ε_0 from the known values of points within a large window of maximum size ε_{max} using the moving average weighting model or kriging:

$$\rho(x_0, \varepsilon_0) = \sum_{x_i \in \Omega(x_0, \varepsilon_{max})} \lambda(\|x_i - x_0\|) Z(x_i) \qquad [4]$$

where $\lambda(\|x_i - x_0\|)$ is the weighting factor of location x_i, which is a function of the distance from x_i to x_0, $\Sigma[\lambda(\|x_i - x_0\|)] = 1$. The value of λ can be estimated using inverse distance weighting or kriging methods, usually based on a global model that can determine the spatial association of the sample locations. Therefore, the value of the center pixel at a finer resolution ε ($\varepsilon < \varepsilon_0$) can be estimated from

$$\rho(x_0, \varepsilon) = (\varepsilon/\varepsilon_0)^{\alpha(x_0)-E} \sum_{x_i \in \Omega(x_0, \varepsilon_{max})} \lambda(\|x_i - x_0\|) Z(x_i) \qquad [5]$$

The factor $(\varepsilon/\varepsilon_0)^{\alpha(x_0)-E}$ modifies the ordinary average in such a way that if $\alpha(x_0) < E$, then the new result is increased by a factor $(\varepsilon/\varepsilon_0)^{\alpha(x_0)-E}$ given $\varepsilon < \varepsilon_0$, whereas if $\alpha(x_0) > E$, then the new result is reduced by a factor $(\varepsilon/\varepsilon_0)^{\alpha(x_0)-E}$. This modification is reasonable because $\alpha(x) < E$ and $\alpha(x) > E$ correspond to convex and concave properties, respectively, of surface $\rho(x, \varepsilon)$ around the location x. For small pixel size, the average density value $\rho(x, \varepsilon)$ estimated using Eq. [5] with $\alpha(x) < E$ is greater than the estimated value of $\rho(x, \varepsilon_0)$ obtained by Eq. [4], whereas the value of $\rho(x, \varepsilon)$ with $\alpha(x) > E$ is smaller than the estimated value of $\rho(x, \varepsilon_0)$. The model not only involves the spatial association reflected in the calculation of weight λ but also incorporates the singularity characterized by the singularity index $\alpha(x)$. The main advantages of the new model in comparison with other ordinary moving average methods include the use of scaling properties to estimate pixel values with multiple resolutions, and values of pixels that are the function of the local singularity measuring the local structure of the property of the map. This property will be demonstrated with a case study of the concentration value of Ag in lake sediment samples. Equations [4] and [5] are illustrated in Fig. 3.

Results and Discussion

Both the ordinary IDW Eq. [4] and the scaling interpolation method Eq. [5] were applied to map the concentration value of Ag in lake sediments in the entire study area from the 1172 lake sediment samples (925 in the mapping area). Figure 4 shows the map generated from 1172 Ag values by means of ordinary IDW with a search distance of 11 km, minimum number of interpolation points of 12, and an inverse distance decay rate of 2. The resultant map is of pixel size = 1 km (1-km resolution). Figure 5 illustrates the distribution of $\alpha(x)$ values of pixels of 1-km size estimated from a set of average values of Ag calculated in squares of sides ε = 1, 3, 5, 7, 9, and 11 km. For any given pixel (x) on the map, six squares of consecutive sizes

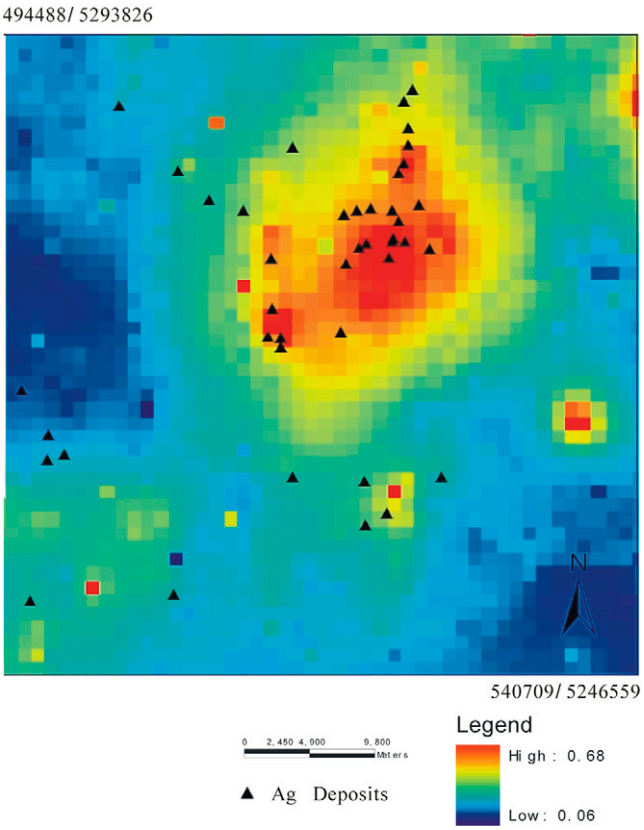


FIG. 4. Results obtained using the inverse distance weighting (IDW) interpolation method for Ag. Pixel size is 1 km, searching distance is 11 km, and inverse distance decay rate was 2.

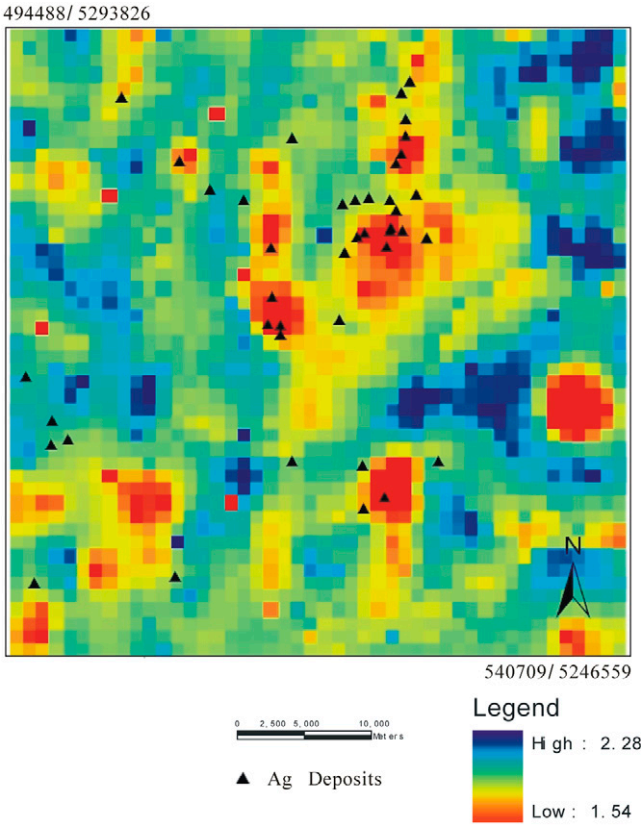


FIG. 5. Distribution of the singularity index α value obtained using Eq. [2] for Ag. Searching scales are 1, 3, 5, 7, 9, and 11 km.

were created and the average values $\mu(x, \varepsilon)$ of Ag were calculated. Then a straight line was fitted to the log-transformed values $\log\mu(x, \varepsilon)$ and $\log(\varepsilon)$. Its slope and intercept were chosen as the $\alpha(x)$ value and $\log(c)$, respectively. The values of the correlation coefficients and standard errors involved in the estimation of the $\alpha(x)$ value are >0.975 and <5%, respectively, for most of the locations, implying that significant linear relationships exist between $\log\mu(x, \varepsilon)$ and $\log(\varepsilon)$. Superimposing the locations of the known Ag deposits on the distribution of $\alpha(x)$ values has shown that most Ag deposits are located in the areas with $\alpha(x) < 2$, which indicates a strong spatial association between the areas of local singularity and the locations of deposits. In many other areas, similar relationships were found between local singularity and locations of mineral deposits of Au, Sn, Cu, Pb, and Zn (Cheng, 2006, 2007a). This type of relationship in a mineral district is common because the areas with low $\alpha(x)$ values may indicate the areas with enriched geochemical values due to mineralization. Comparing the distribution of Ag values in Fig. 4 and the distribution of $\alpha(x)$ values in Fig. 5, we can see that the moving average values shown in Fig. 4 highlight the general trends of the Ag values, which may reflect the general effect of lithology units and structures favorable for Ag mineralization. The distributions usually show continuous and smooth trends that can be interpolated by various methods including kriging and IDW. On the contrary, the anomalous values of $\alpha(x)$ shown in Fig. 5 are the singular component corresponding to a high-pass filtered component that enhances the details related to the local anomalies of Ag mineral deposits. The latter provides a new way to delineate local anomalies caused by mineralization in the fractal space of the α dimension. This has been demonstrated to be effectively useful for delineating favorable targeting areas for further mineral exploration; for example, several areas in the southern part of the map with strong singularity [$\alpha(x) < 2$] but without discovered Ag mineral deposits can be treated as target areas for further exploration. In addition, the following example shows that the local singularity can be used to further interpolate the IDW map to form a finer resolution map. For example, an $\alpha(x)$ value map at a finer resolution, say 200-m resolution, can be formed by moving-averaging the map in Fig. 5. Then according to Eq. [5], with the IDW values in Fig. 4 and the $\alpha(x)$ value at the 200-m resolution, we can generate new values for Ag at a finer resolution, which provides more detail as shown in Fig. 6 (compare with Fig. 4). Similar results were obtained from applying the new data interpolation method to other elements (results not shown).

Conclusions

The scaling interpolation method introduced here can be used for mapping fields and downscaling analysis from point data or an image with local singularity. The processed results using this method contain two separate components: a nonsingular background component with singularity eliminated that can be used for estimation purposes and an anomalous component with strong singularity that can be used for multiscale high-pass filtering purposes. Compared with the ordinary moving average methods, this new method considers the distance between neigh-

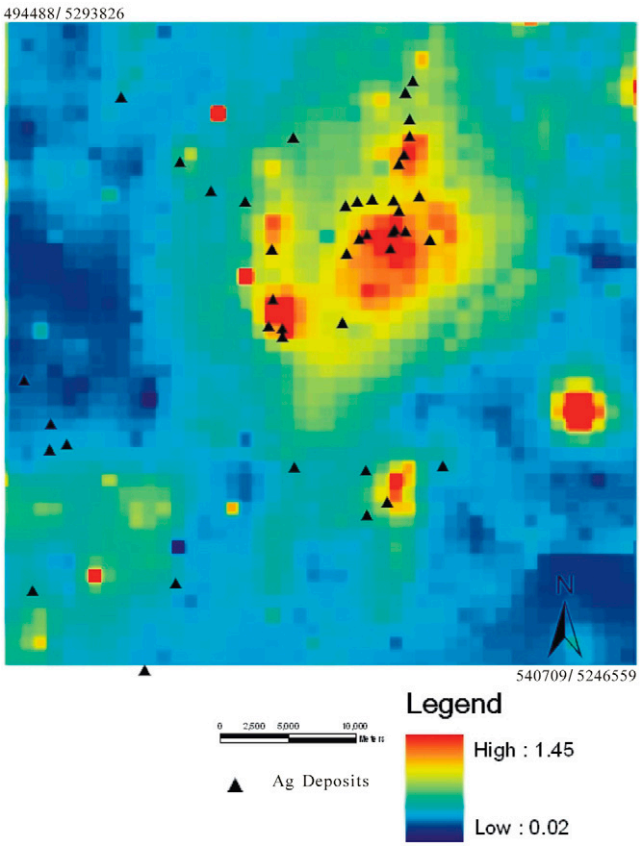


FIG. 6. A map of Ag created using the scaling interpolation model Eq. [5] with values of the constant *c* taken from Fig. 4 and singularity values estimated for pixels of 200-m size. Triangles represent Ag mineral deposits.

borhood point values and takes local structures and singularity into account in assigning weights for data interpolation. This example suggests a new direction for improving interpolation results by utilizing the scaling property quantified by fractal and multifractal models.

ACKNOWLEDGMENTS

Thanks are due to Dr. Alireza Ghaffari for constructive comments. This research has been financially supported by a Distinguished Young Researcher Grant (40525009) and a Strategic Research Grant (40638041) awarded by the Natural Science Foundation of China and a High-Tech Research and Development Grant (2006AA06Z115) by the Ministry of Science and Technology of China.

References

Agterberg, F.P. 1995. Multifractal modeling of the sizes and grades of giant and supergiant deposits. Int. Geol. Rev. 37:1–8.

Agterberg, F.P. 2005. Application of a three-parameter version of the model of de Wijs in regional geochemistry. p. 291–296. *In* Q. Cheng and G.F. Bonham-Carter (ed.) GIS and spatial analysis, Proc. IAMG2005, Toronto. Int. Assoc. Mathmatical Geol., Kingston, ON, Canada.

Andrews, A.J., L. Owsiacki, R. Kerrich, and D.F. Strong. 1986. The silver deposits at Cobalt and Gowganda, Ontario: I. Geology, petrology, and whole-rock geochemistry. Can. J. Earth Sci. 23:1480–1506.

Arneodo, A., F. Argoul, E. Bacry, J. Elezgaray, E. Freysz, G. Grasseau, J.F. Muzy, and B. Pouligny. 1992. Wavelet transform of fractals. p. 287–352. *In* Y. Meyer (ed.) Wavelets and applications: Proc. Int. Conf., Marseille, France. May 1989. Springer-Verlag, Paris.

Arneodo, A., B. Audit, E. Bacry, S. Manneville, J.F. Muzy, and S.G. Roux. 1998. Thermodynamics of fractal signals based on wavelet analysis: Application to fully developed turbulence data and DNA sequences. Physica A 254:24–45.

Arneodo, A., E. Bacry, and J.F. Muzy. 1995. The thermodynamics of fractals revisited with wavelets. Physica A 213:232–275.

Atkinson, P.M., and P. Lewis. 2000. Geostatistical classification for remote sensing: An introduction. Comput. Geosci. 26:361–371.

Badii, R., and A. Politi. 1984. Hausdorff dimension and uniformity of strange attractors. Phys. Rev. Lett. 52:1661–1664.

Badii, R., and A. Politi. 1985. Statistical description of chaotic attractors: The dimension function. J. Stat. Phys. 40:725–750.

Cheng, Q. 1997. Multifractal modeling and lacunarity analysis. Math. Geol. 29:919–932.

Cheng, Q. 1999a. Multifractal interpolation. p. 245–250. *In* S.J. Lippard et al. (ed.) Proc. Annu. Conf. Int. Assoc. for Mathematical Geol., Trondheim, Norway. 6–11 Aug. 1999. Vol. 1. Norw. Univ. of Sci. and Technol., Trondheim.

Cheng, Q. 1999b. Multifractality and spatial statistics. Comput. Geosci. 25:949–961.

Cheng, Q. 2000. Interpolation by means of multiftractal, kriging and moving average techniques. *In* GeoCanada 2000, Proc. GAC/MAC Meeting, Calgary, AB, Canada [CD-ROM]. 29 May–2 June 2000. Geol. Assoc. Can., St. John's, NF, Canada.

Cheng, Q. 2001. A multifractal and geostatistical method for modeling geochemical map patterns and geochemical anomalies. (In Chinese with English abstract.) J. Earth Sci. 26:161–166.

Cheng, Q. 2004. A new model for quantifying anisotropic scale invariance and for decomposition of mixing patterns. Math. Geol. 36:345–360.

Cheng, Q. 2006. A new model for incorporating spatial association and singularity in interpolation of exploratory data. p. 1017–1026. *In* D. Leuangthong and C.V. Deutsch (ed.) Geostatistics Banff 2004. Quantitative Geol. and Geostat. 14. Springer, New York.

Cheng, Q. 2007a. Mapping singularities with stream sediment geochemical data for prediction of undiscovered mineral deposits in Gejiu, Yunnan Province, China. Ore Geol. Rev. 32:314–324.

Cheng, Q. 2007b. Multifractal imaging filtering and decomposition methods in space, Fourier frequency, and eigen domains. Nonlinear Processes Geophys. 14:293–303.

Cheng, Q., and F.P. Agterberg. 1996. Multifractal modeling and spatial statistics. Math. Geol. 28:1–16.

Cheng, Q., and F.P. Agterberg. 2008. Singularity analysis of ore-mineral and toxic trace elements in stream sediments. Comput. Geosci. (in press).

Cheng, Q., F.P. Agterberg, and S.B. Ballantyne. 1994. The separation of geochemical anomalies from background by fractal methods. J. Explor. Geochem. 51:109–130.

ESRI. 2000. ArcMap, Annual of ArcGIS. ESRI, Redlands, CA.

Evertsz, C.J.G., and B.B. Mandelbrot. 1992. Multifractal measures. p. 922–953. *In* H.-O. Peitgen et al. (ed.) Chaos and fractals. Springer, New York.

Feder, J. 1988. Fractals. Plenum Press, New York.

Frisch, U., and G. Parisi. 1985. On the singularity structure of fully developed turbulence. p. 84–88. *In* M. Ghil et al. (ed.) Turbulence and predictability in geophysical fluid dynamics and climate dynamics. North-Holland, New York.

Grassberger, P. 1983. Generalized dimensions of strange attractors. Phys. Lett. A 97:227–230.

Halsey, T.C., M.H. Jensen, L.P. Kadanoff, I. Procaccia, and B.I. Shraiman. 1986. Fractal measures and their singularities: The characterization of strange sets. Phys. Rev. A 33:1141–1151.

Hamilton, S.M. 1997. A high density lake sediment and water geochemical survey of 32 geographic townships in the Montreal River headwaters area, centered on Gowganda area. Open File Rep. 5962. Ontario Geol. Surv., Sudbury, ON, Canada.

Hentschel, H.G.E., and I. Procaccia. 1983. The infinite number of generalized dimensions of fractals and strange attractors. Physica D 8:435–444.

Herzfeld, U.C. 1993. A method for seafloor classification using directional variogram, demonstrated for data from the western flank of the Mid-Atlantic Ridge. Math. Geol. 25:901–924.

Herzfeld, U.C., and C.A. Higginson. 1996. Automated geostatistical seafloor classification: Principles, parameters, feature vectors, and discrimination criteria. Comput. Geosci. 22:35–52.

Journel, A.G., and Ch.J. Huijbregts. 1978. Mining geostatistics. Academic Press, New York.

Li, Q., and Q. Cheng. 2001. Fractal correction of well logging curves. J. China Univ. Geosci. 12:272–275.

Malamud, B.D., D.L. Turcotte, and C.C. Barton. 1996. The 1993 Mississippi River flood: A one hundred or a one thousand year event? Environ. Eng. Geosci. 2:479–486.

Malamud, B.D., D.L. Turcotte, F. Guzzetti, and P. Reichenbach. 2004. Landslide inventories and their statistical properties. Earth Surf. Processes Landforms 29:687–711.

Mandelbrot, B.B. 1972. Possible refinement of the lognormal hypothesis concerning the distribution of energy dissipation in intermittent turbulence. p. 333–351. *In* M. Rosenblatt and C. Atta (ed.) Statistical models and turbulence. Lecture Notes in Physics 12. Springer, New York.

Mandelbrot, B.B. 1974. Intermittent turbulence in self-similar cascades: Divergence of high moments and dimension of the carrier. J. Fluid Mech. 62:331–358.

Mandelbrot, B.B. 1989. Multifractal measures, especially for the geophysicist. Pure Appl. Geophys. 131:5–42.

Panahi, A., Q. Cheng, and G.F. Bonham-Carter. 2003. Modelling lake sediment geochemical distribution using principal component, indicator kriging and multifractal power-spectrum analysis: A case study from Gowganda, Ontario. Geochem. Explor. Environ. Anal. 4:1–12.

Rudin, W. 1988. Real and complex analysis. 3rd ed. Prentice Hall, New York.

Schertzer, D., and S. Lovejoy. 1987. Physical modeling and analysis of rain and clouds by anisotropic scaling of multiplicative processes. J. Geophys. Res. 92:9693–9714.

Sornette, D. 2004. Critical phenomena in natural sciences: Chaos, fractals, self-organization, and disorder. 2nd ed. Springer, New York.

Sullivan, D.G., J.N. Shaw, and D. Rickman. 2005. IKONOS imagery to estimate surface soil property variability in two Alabama physiographies. Soil Sci. Soc. Am. J. 69:1789–1798.

Turcotte, D.L. 1997. Fractals and chaos in geology and geophysics. 2nd ed. Cambridge Univ. Press, Cambridge, UK.

Veneziano, D. 2002. Multifractality of rainfall and scaling of intensity–duration–frequency curves. Water Resour. Res. 38:1–12.

Xie, S., and Z. Bao. 2004. Fractal and multifractal properties of geochemical fields. Math. Geol. 36:847–864.